JACC Vol. 8, No. 3
September 1986:675–81

R and S Wave Changes Produced by Experimental Nontransmural and Transmural Myocardial Infarction

DAVID M. MIRVIS, MD, LESLIE A. INGRAM, MS, KODANGUDI B. RAMANATHAN, MD, FACC, JACK L. WILSON, PHD

Memphis, Tennessee

Electrocardiographic R and S wave changes occur after transmural myocardial infarction. It was the purpose of this study to define the spatial characteristics of these changes and their pathologic determinants after nontransmural as well as transmural necrosis. Twenty-six dogs were studied after occlusion of the left circumflex coronary artery for 60 to 240 minutes, followed by reperfusion. Electrocardiographic potentials were recorded before and 1 week after infarction using an 84 electrode array to compute maximal and root-mean-square R and S wave voltages. Infarct size was quantitated by computer-aided evaluation of heart slices stained by triphenyltetrazolium chloride.

R and S wave amplitudes after infarction varied widely from one torso site to another in a pattern generally consistent with the inferoposterior location of the infarcted zones. Although changes in peak R and S wave potentials did not significantly correlate with infarct size, differences in pre- and postocclusion root-mean-square R and S wave amplitudes did, with correlation coefficients of −0.79 and −0.63, respectively. Root-mean-square values increased for small lesions and decreased for larger ones. These data indicate that nontransmural as well as transmural infarction can produce R and S wave changes that are dependent on overall lesion size and the specific lead studied. Such changes may represent useful methods to quantitate lesion size.

(J Am Coll Cardiol 1986;8:675–81)

It has been known for several decades that QRS changes follow nontransmural as well as transmural infarction. Evolution of Q waves after nontransmural lesions has been consistently reported in clinical and experimental studies. For example, Wilson et al. (1), in 1935, recorded epicardial QR waves from sites in which "the outer layers of muscle were alive and were responding to the excitatory process." R wave changes have similarly been demonstrated after nontransmural infarction. Pruitt et al. (2), in 1945, reported loss of R wave voltage after experimental subendocardial infarction; they subsequently described similar findings in clinical cases in 1958 (3,4). Other experimental and clinical studies (5–8) have reached identical conclusions.

In a prior study (9), we examined the pathologic determinants of new Q wave development after experimental nontransmural and transmural myocardial infarction. Overall infarct size and average transmural extent of necrosis were the two independent predictors that we identified. In the present study, we sought to extend these observations by evaluating the spatial characteristics and the pathologic determinants of the alteration in R and S wave amplitudes after coronary occlusion.

Methods

Experimental model. Twenty-six adult, healthy mongrel dogs were studied. We first performed a left thoracotomy under sterile conditions using a mixture of halothane, nitrous oxide and oxygen. We then placed a hydraulic vascular occluder (4.0 mm internal diameter) around the proximal left circumflex coronary artery. Tubing was then tracked to the back of the neck and buried in a subcutaneous pocket. The chest wall was closed under a water seal and the animal was permitted to recover. We routinely administered acepromazine as an analgesic in addition to broad spectrum antibiotic therapy during the immediate postoperative period.

One week after surgery, we sedated the animals with fentanyl and droperidol (Innovar-Vet, 1 to 2 cc, intramuscular injection) and inflated the implanted balloons by man-

From the Medical Service, Memphis Veterans Administration Medical Center and Departments of Medicine and Anatomy, University of Tennessee College of Medicine, Memphis, Tennessee. This project was supported by research grants from the Veterans Administration, Washington, DC and Grant HL20597 from the National Heart, Lung, and Blood Institute, Bethesda, Maryland.

Manuscript received December 3, 1985; revised manuscript received February 25, 1986, accepted March 19, 1986.

Address for reprints: David M. Mirvis, MD, 956 Court Avenue, Room F208, Memphis, Tennessee 38163.

©1986 by the American College of Cardiology

0735-1097/86/$3.50

ual injection of mineral oil until we encountered significant resistance to further infusion. Occlusion was maintained by clamping the tubing for 60 minutes in six dogs, 90 minutes in eight dogs, 2 hours in eight dogs and 4 hours in the remaining four dogs. At the end of the designated period, we aspirated the oil from the occluder and left the tubing open to atmospheric pressure. This occlusion-reperfusion model has been demonstrated to yield a range of infarct sizes, varying directly with the duration of occlusion (10).

Electrocardiographic recordings. We recorded electrocardiographic potentials twice for each dog. The first data set was acquired 1 week after thoracotomy and immediately before balloon inflation. By this time, the qualitative effects of thoracotomy on the surface electrocardiogram had largely resolved (11). The second set of potentials was registered 1 week later.

Before each recording period, we sedated the dogs. An electrode grid, consisting of 84 chloridized silver discs, was then fixed to the shaven torso in 14 strips of six electrodes that extended from the level of the clavicles to below the inferior rib margins. Two-thirds of the electrodes were on the anterior and one-third were on the posterior torso surfaces. Electrode strip locations were marked to assure reproducible positioning for both recording sessions. The animals were then suspended in an upright posture using a support sling. Additional electrodes were placed on the limbs to record the standard and augmented limb leads and to derive the Wilson central terminal potential.

Potentials from each of the 88 electrodes were amplified by low noise, differential (versus Wilson central terminal potential) amplifiers with gains of 1,000 to 16,000. The gain of each channel was individually set so that the amplifier output filled the input range of the analog to digital convertor. Analog data were then converted to digital form at the rate of 500 samples/channel per second.

Electrocardiographic data analysis. Fourteen seconds of electrocardiographic data were stored for off-line analysis. First, PQRST waveforms of similar form, as determined by an autocorrelation method (12), were averaged to reduce random noise. We then manually selected the beginning and end of the PR, QRS and ST-T intervals from expanded plots of three relatively orthogonal leads. Potentials during a 10 ms interval of the terminal TP segment were averaged to provide a zero potential reference level.

We then quantitated the following variables from each electrode waveform: 1) the maximal R wave amplitude, and 2) the maximal S wave depth. These values, determined at each of the 84 torso locations, were then processed to construct isopotential body surface maps by connecting sites with equal magnitudes. Difference maps were constructed by subtracting the values recorded before from those recorded after infarction.

In each preocclusion, postocclusion and difference map, the greatest R wave amplitude and the greatest S wave depth in the 84 lead waveforms were determined. In addition, the root-mean-square values for each of the variables in preocclusion and postocclusion data sets were computed using the equation:

$$RMS_n = \sqrt{V_i^2/84},$$

where RMS_n = the root-mean-square value of variable n (R, S amplitude) and V_i = the value of variable n in electrode recording i. This value corresponds to the magnitude of the variable at any arbitrary torso location.

Infarct size measurement. Immediately after the second recording session, the animal was killed by injection of potassium chloride. We rapidly excised the heart and sliced it into 8 mm sections parallel to the base using a brain macrotome. The sections were incubated in triphenyltetrazolium chloride (1% solution in phosphate buffer) for 30 minutes at 37°C to delineate necrotic tissue (13).

Photographs of the slices were traced onto a microcomputer-based graphics digitizing tablet. From these traces, the following variables were quantitated: 1) the percent of the left ventricle that was infarcted, using Simpson's rule to calculate areas and a paraboloid model of the left ventricle to calculate volumes (14); 2) the maximal and average transmural depth of the infarction, expressed as a percent of wall thickness; and 3) the percent of each of five concentric layers of the ventricular wall that was necrotic (9). To compute the latter, the ventricular wall was subdivided into five segments of equal thickness, with segment 1 being on the endocardial and segment 5 being on the epicardial surface. Each segment was bordered laterally by radii drawn from the geometric centroid of the left ventricular cavity to the endocardial margins of the infarct, and extended through the ventricular wall. We defined a transmural lesion as one with greater than 10% necrosis in the outermost segment.

Statistical analysis. All quantitated data are presented as mean ± 1 SD. Comparisons between groups relied on analysis of variance with a 5% level of significance. We utilized a stepwise multiple linear regression model (15) to determine which anatomic variables were statistically significant, independent determinants of the electrocardiographic measures. Variables were added to or deletd from the model using an F ratio test.

Results

Infarct size measurements. The wide range of lesion dimensions produced is documented in Table 1. Detectable areas of infarction did not develop in four dogs. These cases served to quantitate the effects of time alone on the electrocardiographic variables. In the remaining 22 animals, from 0.33 to 36.5% of the left ventricle was rendered necrotic. Lesions were transmural in four cases and nontransmural in the remaining 18 animals.

Table 1. Infarct Size Measurements (n = 22)*

Variable	Mean ± SD	Range
Percent left ventricle infarcted	11.3 ± 10.4	0.3 to 36.5
Average transmural depth	39.7 ± 19.7	11.1 to 77.8
Maximal transmural depth	86.3 ± 21.7	25.4 to 100.0
Transmural segment infarcted		
1	54.7 ± 17.5	19.5 to 88.5
2	42.5 ± 19.3	2.4 to 81.1
3	29.2 ± 23.2	0.0 to 71.7
4	19.1 ± 22.7	0.0 to 72.5
5	12.7 ± 24.9	0.0 to 73.9

*Includes only cases with demonstrated infarction. All values are in percent.

R wave and S wave amplitudes. In the four animals that did not develop infarction, the magnitudes of the peak R and S amplitudes varied by less than 10% between the two recording periods. Differences in the root-mean-square values for the R and S wave potentials differed by 28.5 ± 35.3 and 31.1 ± 37.4 μV, respectively, between the pre- and postocclusion data sets. Thus, changes during the 2 week interrecording period in cases without infarction were small.

In those dogs that did have zones of necrosis, however, the amplitudes varied widely at different torso sites in any one animal and among different experimental animals. This spatial variability is shown in the isopotential maps of Figures 1 and 2. In each map, the plus and minus signs indicate electrode positions, with the sign corresponding to the polarity of the sensed voltage. The center of each map is along the sternum; the right and left edges then correspond to the left and right paravertebral zones, respectively. Contour lines connect sites at equal potential relative to that of the Wilson central terminal. Zero lines are overdrawn for emphasis. Sites with the most positive (maximal) and most negative (minimal) potentials are boxed, and the magnitudes of these values are listed in each frame.

In the case shown in Figure 1, 24.6% of the left ventricle was necrotic after 120 minutes of circumflex artery occlusion. Only 2.6% of the outermost one-fifth of the ventricle was necrotic; hence, we classified the lesion as nontransmural. R wave patterns before and after infarction are shown in Figure 1A and B, respectively. Before coronary occlusion, the maximal R wave potential measured 2,865 μV and was recorded from a site on the left anterior chest. The tallest R waves were usually registered from electrodes on the anterior inferior surface. One week after occlusion (Fig. 1B), the tallest R wave measured 2,268 μV; a change in the spatial R wave pattern occurred with a superior shift of sites with the highest potentials.

Changes in R wave potentials after infarction are highlighted in the difference map in Figure 1C, computed by subtraction of values in Figure 1A from those in Figure 1B.

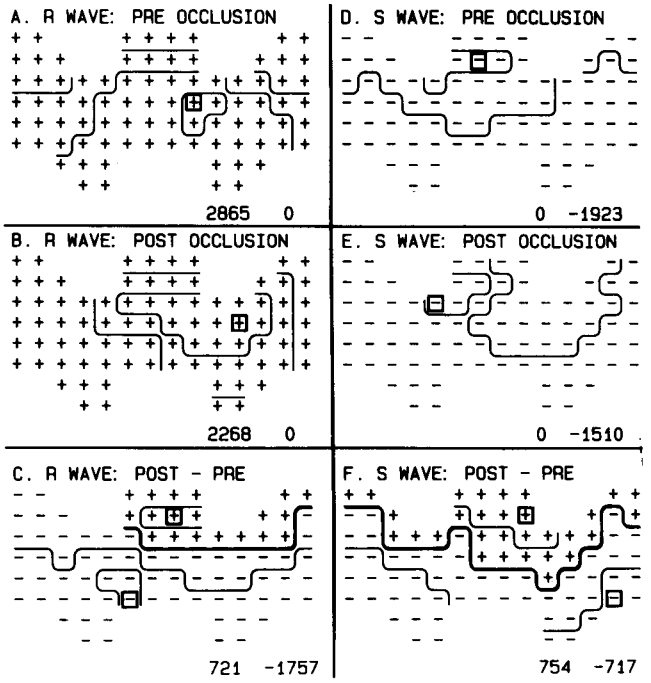

Figure 1. Body surface isopotential maps depicting the spatial distribution of peak R wave and S wave voltages before and after occlusion of the left circumflex artery. **Markings** in each panel are as detailed in the text (see Results section). Peak R wave patterns before and after 2 hours of arterial occlusion are shown in **A** and **B**, respectively. Corresponding peak S wave distributions are demonstrated in **D** and **E**. Difference maps in **C** and **F** were computed by subtraction of preocclusion (**A** or **D**) from postocclusion (**B** or **E**) patterns. **Contour lines** are drawn at 0 and at ± 500, 1,500 and 2,500 μV levels. Sites with the most positive (maximal) and most negative (minimal) potentials are **boxed,** and the magnitudes of these values are listed in each frame.

Figure 2. Isopotential difference maps depicting the change in peak R wave (**A**) and peak S wave (**B**) potentials after 60 minutes of circumflex artery occlusion. All **markings** are as in Figure 1.

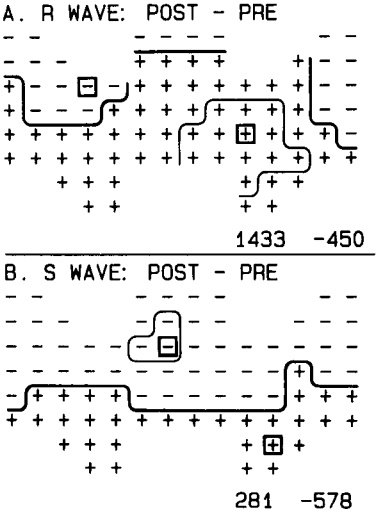

R wave potentials over most of the inferior torso were reduced (negative values in difference map) after infarction, whereas those on the superior surface were augmented (positive values in difference map). Thus, nontransmural infarction altered R wave magnitudes in a spatial, or lead-dependent, manner. Zones of reduced amplitude corresponded to the expected torso region from which potentials of the circumflex artery bed would be projected. Root-mean-square R wave potential measured 1,525.1 before and 1,208.0 μV after infarction.

Maps in Figure 1D to F show the effects of this nontransmural infarction on S wave depth. Before occlusion (Fig. 1D), the deepest (most negative) S waves were recorded from sites on the superior torso. After infarction (Fig. 1E), peak S wave depth was reduced from $-1,923$ to $-1,510$ μV. As shown in the difference map of Figure 1F, representing the difference between Figure 1D and E, S waves over the inferior torso became deeper (that is, more negative), whereas those on the superior torso became less deep (that is, less negative). S wave root-mean-square potentials measured 678.5 and 484.7 μV before and after infarction, respectively. Zones of directional S and R wave changes generally corresponded, such that R and S waves became more negative over the inferior torso.

Distributions from a second case with a nontransmural infarction occupying only 8.2% of the left ventricle are shown in Figure 2. Maps in Figure 2A and B are R and S wave difference maps, respectively. In this case, R waves over much of the chest but especially over the inferior surface were augmented (Fig. 2A), whereas S waves over a similar region were made less negative (Fig. 2B) by the infarction. R and S wave root-mean-square potentials increased by 286.3 and 84.7 μV, respectively, after infarction. Thus, the spatial patterns in this case were in directions opposite to those of the example presented in Figure 1.

Changes in peak maximal R and S wave potentials varied from 197.3 to 1,521.1 and 170.6 to 649.8 μV, respectively. Corresponding ranges for the changes in root-mean-square R and S wave potentials equaled -634.8 to 376.9 and -172.7 to 228.5 μV, respectively. QRS duration increased by 0.27 $\pm$ 3.05 ms ($p > 0.05$) after infarction.

Electrocardiographic-pathologic correlations. We next attempted to explain such spatial differences as shown in Figures 1 and 2 and the range of computed R and S wave changes by examining correlations between the electrocardiographic variables and the anatomic measurements. Electrocardiographic variables, considered as dependent variables, included 1) differences in the peak R wave and the peak S wave amplitudes before and after infarction, and 2) differences in root-mean-square R wave and root-mean-square S wave potentials before and after infarction. Anatomic measurements, treated as independent variables, included those listed in Table 1.

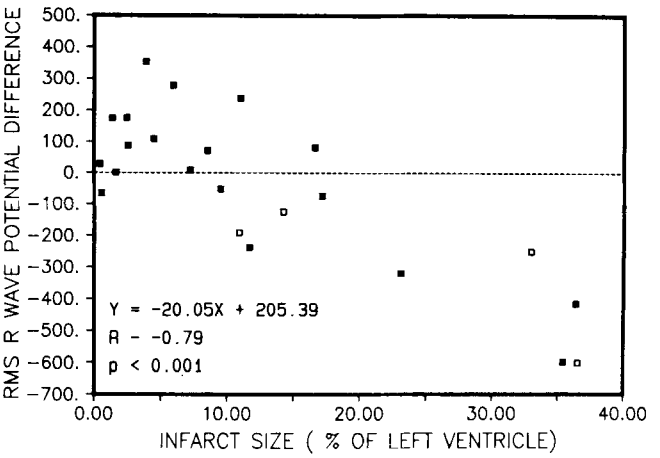

Figure 3. Plot depicting the relation between infarct size, expressed as the percent of left ventricle that was necrotic, and the difference between pre- and postocclusion R wave root-mean-square (RMS) potential. The computed regression equation and correlation coefficient are listed. **Solid squares** identify nontransmural lesions and **open squares** mark transmural ones.

Changes in the maximal R and S wave amplitudes did not significantly correlate with any of the anatomic infarct variables. The highest correlation coefficient computed was 0.31 ($p > 0.05$).

In contrast, changes in root-mean-square R and S wave potentials correlated significantly with infarction size measures. A plot of root-mean-square R wave potential difference as a function of infarct size is shown in Figure 3. A strong linear correlation ($r = 0.79$) existed between these two variables. Smaller lesions resulted in an increase in root-mean-square potential, whereas larger ones produced a decrease in that value. Very small areas of necrosis (<3% of left ventricle) produced little change, that is, within con-

Figure 4. Plot, as in Figure 3, of the relation between changes in S wave root-mean-square (RMS) potential and infarct size. Nontransmural lesions are marked by **solid squares** and transmural ones by **open squares.**

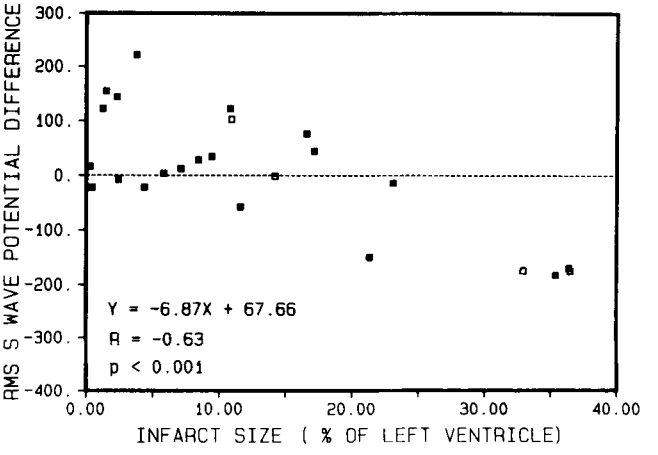

fidence limits of changes observed in cases without infarction. A similar although less rigorous relation existed between infarct size and the change in root-mean-square S wave potential (Fig. 4). The R and S wave regression equations for nontransmural and transmural lesions were colinear; that is, their slopes and intercepts were not significantly different ($p > 0.05$).

Correlation coefficients between the root-mean-square changes and other infarct size variables are listed in Table 2. For R wave changes, inversely correlated variables included average transmural depth and the percent necrosis in the four outer fifths of the ventricular wall. For S wave values, only average depth and percent infarction in the most epicardial (fifth) wall were significantly correlated.

Finally, we sought to determine which of the anatomic variables were statistically significant, independent determinants of root-mean-square R and S wave potentials. To do this, we relied on a stepwise multiple linear regression model. For each wave, only the percent of the left ventricle that was necrotic was shown to be of independent predictive value. Other anatomic variables that individually did correlate with potential changes (Table 2) did not add significant, independent information.

Discussion

The findings of this study demonstrate that 1) experimental nontransmural and transmural infarctions do alter R and S wave potentials, and 2) the magnitudes and directions of these QRS potential changes are largely determined by the size of the necrotic lesion.

Prior studies. As noted earlier, it has been suggested for some time that nontransmural lesions may produce virtually all of the QRS changes usually attributed to transmural infarction. Although most recent reports, as well as older clinical and experimental studies, have emphasized the determinants of Q wave patterns (7–9), some investigators (2–4) have attempted to prove that mid and late QRS changes also follow nontransmural lesions. Pruitt et al. (2) and Prinzmetal et al. (5) reported reduced precordial and epicardial R waves, respectively, after experimental chronic or acute subendocardial injury. Their work did not, however, characterize the changes or quantitatively relate them to the responsible pathologic features.

Table 2. Correlation Coefficients Between Infarct Size Variables and R and S Wave Root-Mean-Square Potential Differences

Variable	R Wave	S Wave
Percent left ventricle infarcted	−0.79	−0.63
Average transmural depth	−0.62	−0.44
Maximal transmural depth	NS	NS
Transmural segment infarcted		
1	NS	NS
2	−0.49	NS
3	−0.62	NS
4	−0.63	NS
5	−0.54	−0.51

NS = not statistically significant, $p > 0.05$.

R and S wave changes. Our present data clearly substantiate the ability of nontransmural lesions to alter R and S wave amplitudes. The specific nature of the alterations was complex, varying with electrode location and lesion size. First, the direction and magnitude of the R and S wave changes varied from one torso site to another. They are, therefore, lead-dependent effects. For example, peak R wave potentials increased over the superior torso in the example shown in Figure 1, whereas they decreased in inferior positions. These spatial effects, clearly demonstrated by isopotential mapping techniques (16), topographically relate to the location of infarction within the chest. The inferior-superior axis of the alterations shown in Figures 1 and 2 correlates with the inferior, posterior and lateral location of the circumflex artery perfusion territory (17). This is the same distribution previously documented for Q wave changes after circumflex artery occlusion (9). Thus, when assessing QRS changes, the lead axis and strength in relation to lesion location must be considered. It is also conceivable, or even likely, that direct epicardial leads could identify QRS changes not transmitted to the body surface (18).

The second feature of the R and S wave changes was the dependence on lesion size. Whereas large infarcts reduced root-mean-square R and S wave voltage, smaller ones increased these values. The observed increase in root-mean-square potential after infarction in the small and moderate size lesions (Fig. 3 and 4) may seem paradoxical; a reduction in potential would be expected with loss of muscle mass (1,19,20). One explanation for this finding relates to the prominent effects of cancellation of electrical forces by simultaneously active effects oriented in opposite directions. Reduction of the force of one of these competing effects might then increase rather than decrease the observed surface potentials. This notion has been proposed by Flowers et al. (21) to explain the development of mid and late QRS changes after clinical infarction. To provide evidence for this consideration, we performed a simple numerical simulation of the hypothesized conditions (see Appendix).

Pathologic correlations of R and S wave changes. As detailed earlier, a wide range of R and S wave changes were observed; the variation was in both direction and magnitude. One possible explanation for this was an effect predicted by anatomic variables. We therefore performed the electrocardiographic-pathologic correlations described before.

Two results of this effort were significant. First, postinfarction changes in peak R and S wave amplitude were not significantly related to lesion size, whereas changes in

root-mean-square potentials were (Table 2). The explanation for this difference may also reside in the spatial effects included within a root-mean-square measure. Potentials from all torso sites are included within the root-mean-square equation, permitting a greater sensitivity to spatial myocardial variables. In addition, by including measures from all rather than from only one torso site, the root-mean-square values minimize the effects of altered orientation of electrical forces. A similar relation has been reported by Burgess et al. (22) in a study of epicardial heating; the sum of QRST area changes correlated with the area warmed, whereas peak changes related to the intensity of the temperature change. It is the former that is analogous to infarct size.

Second, infarct size, which we quantitated as the percent of the left ventricle made necrotic, was the only anatomic variable that had significant and independent value for predicting root-mean-square changes. Other pathologic measures were significantly correlated with the electrocardiographic effects, but none provided correlative information not supplied by lesion size alone. This measure was also the major, although not the sole, determinant of the new Q waves. Thus, development of Q wave as well as R and S wave changes after nontransmural infarction has similar determining factors, that is, infarct size.

Clinical implications. Thus, nontransmural infarctions do result in QRS changes that are related, in specific ways, to lesion extent. Factors of possible clinical relevance then include the recognition that R or S wave changes after infarction do not necessarily denote a transmural lesion, but probably reflect a large necrotic zone with variable transmural extension. This is directly analogous to the significance of new Q waves (9). Assessing these R and S wave effects must, however, include consideration of the specific electrocardiographic formulation and lead used.

The highly significant correlation between root-mean-square R and S wave changes and lesion size (Fig. 3 and 4) further suggests that such measures may be useful for quantitating infarct size. R and S wave changes after transmural infarction have been so utilized (23,24). The present data suggest that such effects may be of value in lesions of both nontransmural and transmural form. These implications must, however, be considered only in view of the real and significant differences between the clinical environment and our experimental models.

Appendix

Simulation Studies

Two dipoles were placed within a bounded homogeneous sphere (Fig. 5A) with a radius of 3.175 cm. The dipoles were radially oriented at an eccentricity of 0.25 and separated by angles of 90, 135 or 180°. The total moment of the first dipole (M_1) was fixed at 10,000 μA cm/Ω cm, whereas that of the second (M_2) was varied from 10,000 to 0 μA cm/Ω cm. These diploes are generally equivalent to the forces created by two uniform double layers (25), such as those produced by infarction zones. Potentials at each of 32 surface electrodes distributed symmetrically on the surface of the sphere were computed (26). Root-mean-square potentials were then calculated as described in the Methods section.

Results of this simulation are shown in Figure 5B. When the two dipoles were 90° apart, decreasing the strength of one dipole from 10,000 to 0 μA cm/Ω cm progressively reduced the surface root-mean-square potential. However, when the angle between the

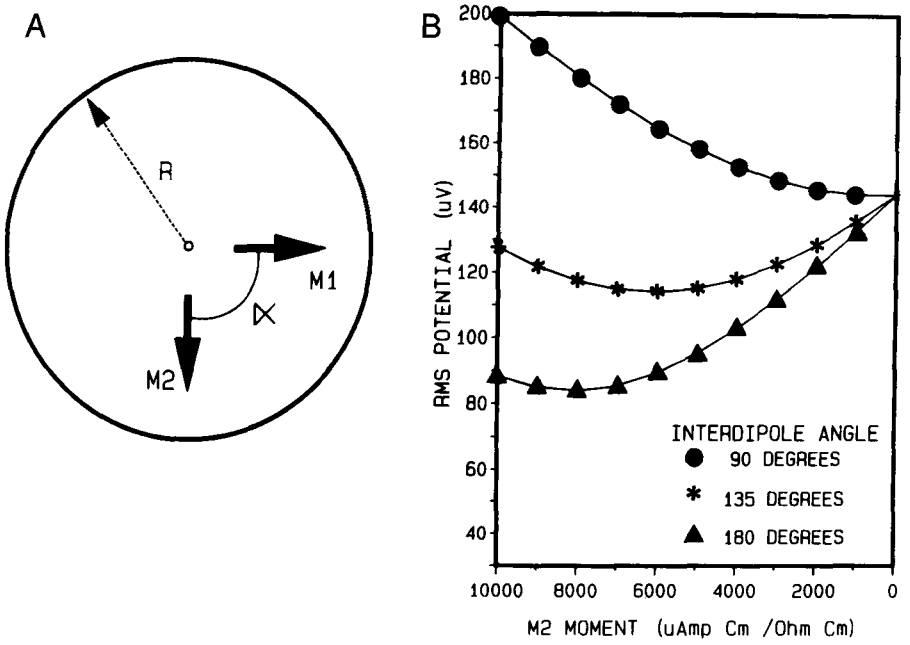

Figure 5. A, Representation of the simulation model described in the text. R is the radius (3.175 cm) of the bounded sphere. The two dipoles, M_1 and M_2, are radially oriented at an eccentricity of 0.25, that is, located R/4 cm from the center of the sphere. The interdipole angle alpha (α) is the angle between the two dipoles. **B,** Effects of reducing the moment of dipole M_2 in **A** from 10,000 to 0 μA cm/Ω cm on surface root-mean-square (RMS) potential. Moment of M_1 was maintained at 10,000 μA cm/Ω cm. Plots are shown for three interdipole angles, alpha.

vectors was increased to 135 or 180°, the surface root-mean-square voltage when both M_1 and M_2 were set at 10,000 μA cm/Ω cm was less than that at 90°; reducing the moment of the second dipole (M_2) increased the surface root-mean-square voltage after an initial decrease. This effect was greater at 180 than at 135°.

The lesser potential when the two equipotent dipoles were farther apart is a direct reflection of cancellation of oppositely directed forces. As the strength of one was reduced, so was the degree of cancellation, and root-mean-square surface potential increased. Thus, reducing the strength of cardiac vectors, such as by myocardial infarction, may produce a seemingly paradoxical increase in body surface electrocardiographic voltages. Probably additional factors interact with this one in in vivo infarction. For example, conduction delay produced by ischemia or infarction, or both, will also produce R wave augmentation, as shown by David et al. (27). Reduction in root-mean-square forces with larger lesions probably reflects the predominant effects of muscle mass loss.

References

1. Wilson FW, Hill IGW, Johnston FD. The form of the electrocardiogram in experimental myocardial infarction. III. The later effects produced by ligation of the anterior descending branch of the left coronary artery. Am Heart J 1935;10:903–15.
2. Pruitt RD, Barnes AR, Essex HE. Electrocardiographic changes associated with lesions in deeper layers of myocardium: experimental study. Am J Med Sci 1945;210:100–18.
3. Cook RW, Edwards JE, Pruitt RD. Electrocardiographic changes in acute subendocardial infarction. I. Large subendocardial and large transmural infarcts. Circulation 1958;19:603–12.
4. Cook RW, Edwards JE, Pruitt RD. Electrocardiographic changes in acute subendocardial infarction. II. Small subendocardial infarcts. Circulation 1958;18:613–22.
5. Prinzmetal M, Shaw McK, Maxwell MH, et al. Studies on the mechanism of ventricular activity. VI. The depolarization complex in pure subendocardial infarction: role of the subendocardial region in the normal electrocardiogram. Am J Med 1954;17:469–89.
6. Beller GA, Hood WB, Smith TW. Effects of ischemia and coronary reperfusion on regional myocardial blood flow and on the epicardial electrogram. Cardiovasc Res 1977;11:489–98.
7. Spodick DH. Q-wave infarction versus S-T infarction. Nonspecificity of electrocardiographic criteria for differentiating transmural from nontransmural lesions. Am J Cardiol 1983;51:913–5.
8. Raunio H, Rissanen V, Romppanen T, et al. Changes in the QRS complex and ST segment in transmural and subendocardial myocardial infarction. Am Heart J 1979;98:176–84.
9. Mirvis DM, Ingram L, Holly MK, Wilson JL, Ramanathan KB. Electrocardiographic effects of experimental nontransmural myocardial infarction. Circulation 1985;71:1206–14.
10. Reimer KA, Lowe JE, Rasmussen NM, Jennings RB. The wavefront phenomenon of ischemic cell death. I. Myocardial infarct size vs. duration of coronary occlusion in dogs. Circulation 1977;56:786–96.
11. Mirvis DM. Effects of thoracotomy on volume conductor properties of the canine torso. J Electrocardiol 1983;16:279–86.
12. Brody DA, Woolsey MD, Arzbaecher RC. Application of computer techniques to the detection and analysis of spontaneous P-wave variations. Circulation 1967;36:359–71.
13. Fishbein MC, Meerbaum S, Rit J, et al. Early phase acute myocardial infarct size quantification: validation of the triphenyl tetrazolium chloride tissue enzyme staining technique. Am Heart J 1981;101:593–600.
14. Ideker RE, Hackel DB, McClees EC. Postmortem-anatomic quantitation. In: Wagner GS, ed. Myocardial Infarction: Measurement and Intervention. Boston: Martinus Nijhoff, 1982:347–71.
15. Dixon WJ. BMDP Statistical Software. Berkeley, CA: University of California Press, 1983.
16. Mirvis DM, Keller FW, Ideker RE, Cox JW, Zettergren DG, Dowdie RF. Values and limitations of surface isopotential mapping techniques in the detection and localization of multiple discrete epicardial events. J Electrocardiol 1977;10:347–58.
17. Scheel KW, Ingram LA, Gordey RL. Relationship of coronary flow and perfusion territory in dogs. Am J Physiol 1982;243:H738–47.
18. Bodenheimer MM, Banka VS, Trout RG, Pasdar H, Helfant RH. Correlation of pathologic Q waves on the standard electrocardiogram and the epicardial electrogram of the human heart. Circulation 1976;54:213–8.
19. Prinzmetal M, Kennamer R, Maxwell M. Studies on the mechanism of ventricular activity. VIII. The genesis of the coronary QS wave in through-and-through infarction. Am J Med 1954;17:610–3.
20. Shaw CMcK, Goldman A, Kennamer R, et al. Studies on the mechanism of ventricular activity. VII. The origin of the coronary QR wave. Am J Med 1954;16:490–503.
21. Flowers NC, Horan LG, Johnson JG. Anterior infarctional changes occurring during mid and late ventricular activation detectable by surface mapping techniques. Circulation 1976;54:906–13.
22. Burgess MJ, Lux RL, Wyatt RF, Abildskov JA. The relation of localized myocardial warming to changes in cardiac electrograms in dogs. Circ Res 1978;43:899–907.
23. Palmeri ST, Harrison DG, Cobb FC, et al. A QRS scoring system for assessing left ventricular function after myocardial infarction. N Engl J Med 1982;306:4–9.
24. Hillis LD, Askenazi J, Braunwald E, et al. Use of changes in the epicardial QRS complex to assess interventions which modify the extent of myocardial necrosis following coronary artery occlusion. Circulation 1976;54:591–8.
25. Brody DA, Bradshaw JC. The equivalent generator components of uniform double layers. Bull Math Biophys 1962;24:183–95.
26. Brody DA, Terry FH, Ideker RE. Eccentric dipole in a spherical medium: generalized expression for surface potentials. IEEE Trans Biomed Eng 1973;20:141–3.
27. David D, Naito M, Michelson EL, et al. Intramyocardial conduction: a major determinant of R-wave amplitude during acute myocardial ischemia. Circulation 1982;65:161–7.